Antarctic Science 33(2), 174–188 (2021) © Antarctic Science Ltd 2020 doi:10.1017/S0954102020000619

Cryostratigraphy of mid-Miocene permafrost at Friis Hills, McMurdo Dry Valleys of Antarctica

MARJOLAINE VERRET [1], WARREN DICKINSON [1], DENIS LACELLE [2], DAVID FISHER [3], KEVIN NORTON [4], HANNAH CHORLEY [1], RICHARD LEVY [1,5] and TIM NAISH [1]

[1] Antarctic Research Centre, Victoria University of Wellington, Wellington, New Zealand
[2] Department of Geography, Environment and Geomatics, University of Ottawa, Ottawa, Canada
[3] Department of Earth Sciences, University of Ottawa, Ottawa, Canada
[4] School of Geography, Environment and Earth Sciences, Victoria University of Wellington, Wellington, New Zealand
[5] GNS Science, Lower Hutt, New Zealand
Marjolaine.Verret@vuw.ac.nz

Abstract: The origin and stability of ground ice in the stable uplands of the McMurdo Dry Valleys remains poorly understood, with most studies focusing on the near-surface permafrost. The 2016 Friis Hills Drilling Project retrieved five cores reaching 50 m depth in mid-Miocene permafrost, a period when Antarctica transitioned to a hyper-arid environment. This study characterizes the cryostratigraphy of arguably the oldest permafrost on Earth and assesses 15 Myr of ground ice evolution using the REGO model. Four cryostratigraphic units were identified: 1) surficial dry permafrost (0–30 cm), 2) ice-rich to ice-poor permafrost (0.3–5.0 m) with high solute load and $\delta^{18}O$ values (-16.2 ± 1.8‰) and low D-excess values (-65.6 ± 4.3‰), 3) near-dry permafrost (5–20 m) and 4) ice-poor to ice-rich permafrost (20–50 m) containing ice lenses with low solute load and $\delta^{18}O$ values (-34.6 ± 1.2‰) and D-excess of 6.9 ± 2.6‰. The near-surface $\delta^{18}O$ profile of ground ice is comparable to other sites in the stable uplands, suggesting that this ice is actively responding to changing surface environmental conditions and challenging the assumption that the surface has remained frozen for 13.8 Myr. The deep ice lenses probably originate from the freezing of meteoric water during the mid-Miocene, and their $\delta^{18}O$ composition suggests mean annual air temperatures ~7–11°C warmer than today.

Received 19 August 2020, accepted 19 October 2020

Key words: ground ice, Miocene Climatic Optimum, soluble ions, stable upland zone, stable water isotopes

Introduction

Ground ice and its evolution in permafrost plays a central role in landscape development. The high elevations of the McMurdo Dry Valleys (MDV), known as the *stable upland* or *ultraxerous* zone (e.g. Marchant & Head III 2007) are thought to have remained frozen under a hyper-arid polar climate since *c.* 13.8 Ma (e.g. Valletta *et al.* 2015). Early numerical modelling suggested that the uppermost tens of metres of permafrost soils in the upper MDV should be largely deprived of ground ice due to its sublimation under a hyper-arid climate (e.g. McKay *et al.* 1998). However, recent investigations of the depth of the interface between dry and icy permafrost (i.e. the ice table) found that 90% of the surveyed sites in the stable uplands had ice-table depths of < 80 cm (e.g. Marinova *et al.* 2013, Fisher *et al.* 2016). Numerous shallow cores (< 6 m) in 100 000 to several million year-old permafrost soils also indicate that ground ice is present, and often above pore saturation, known as excess ice (e.g. Dickinson & Rosen 2003, Lacelle *et al.* 2013, Lapalme *et al.* 2017). In addition to the burial of glacier ice (e.g. Lacelle *et al.* 2011, Swanger 2017), different hypotheses have been advanced to explain the emplacement of ground ice in the icy permafrost of the upper MDV. For example, in places where ground temperatures remain < 0°C, ground ice was probably emplaced by vapour diffusion, whereas in places where ground surface temperatures rise to > 0°C, it was probably emplaced by a combination of vapour diffusion and freezing of evaporated snowmelt (e.g. Dickinson & Rosen 2003, Lacelle *et al.* 2013, Lapalme *et al.* 2017). Therefore, ground-ice conditions in the stable uplands can provide information about past environmental conditions, specifically whether persistent cold and hyper-arid conditions prevailed or whether these climate conditions were interrupted sporadically with the infiltration of liquid water in the dry soil lag and its subsequent freezing in icy permafrost soils.

The Friis Hills inselberg located at ~1500 m above sea level (a.s.l.) in the upper MDV contains a 50 m-thick sequence of stacked glacial drifts interbedded with silty

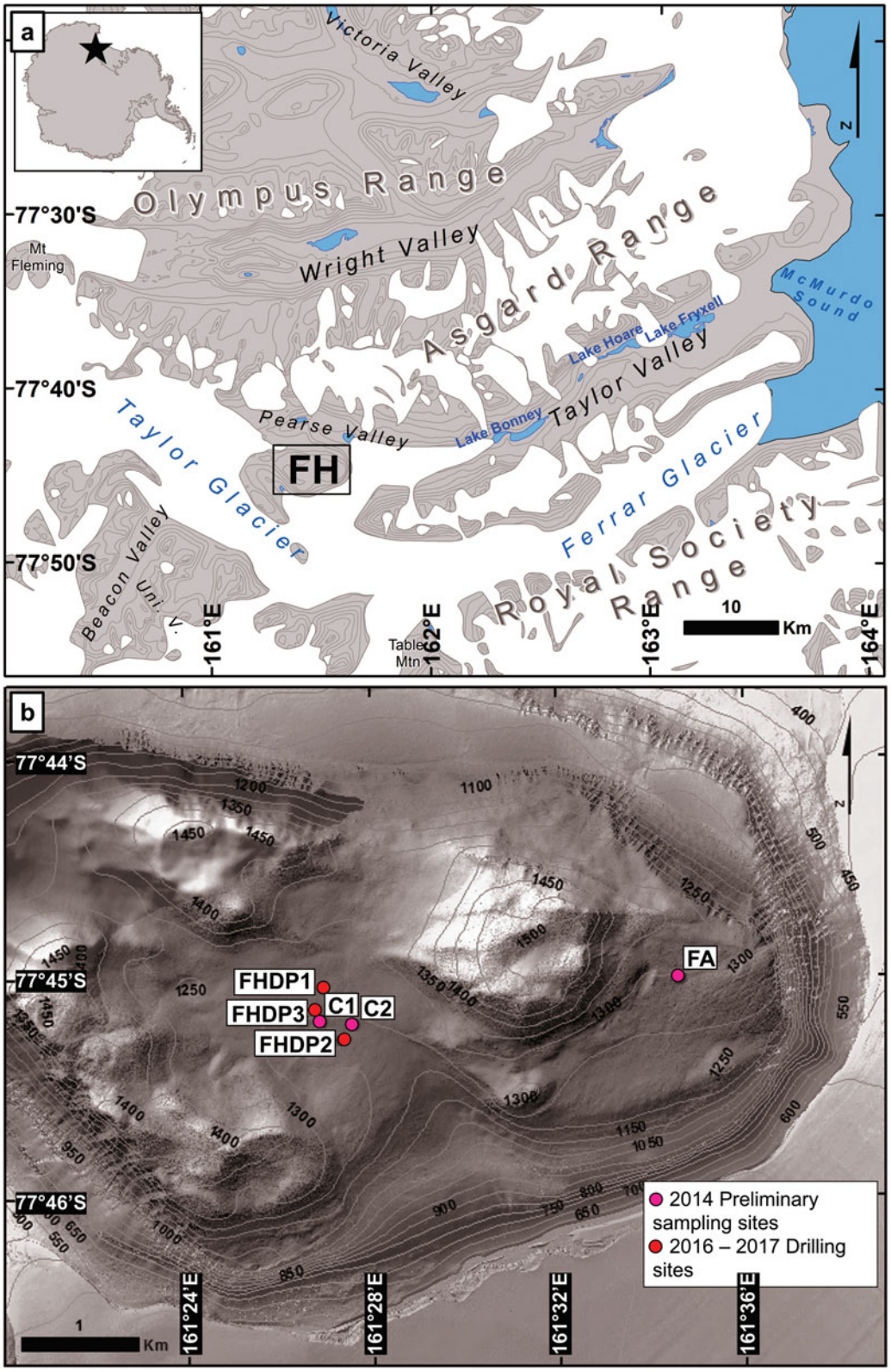

Fig. 1. a. Map showing the location of Friis Hills (FH) in the McMurdo Dry Valleys (contour lines at 200 m intervals) and **b.** topographical map of FH (contour lines at 50 m intervals) with sampling and drilling sites (background LIDAR imagery from Fountain *et al.* 2017).

https://doi.org/10.1017/S0954102020000619 Published online by Cambridge University Press

fluvial and lacustrine sediments (Lewis & Ashworth 2015). The lower drift deposit was dated at 19.7 Ma from a tephra layer, whereas the top of the upper sediments is correlated with an erosional phase at 13.6–12.4 Ma, as observed in other areas in the MDV (Lewis & Ashworth 2015). The period of sediment deposition corresponds to the Miocene Climatic Optimum (MCO; 17–15 Ma) and the progressive cooling of the middle Miocene climate transition (MMCT), which initiated the transition to cold hyper-arid conditions (15–13 Ma; e.g. Flower & Kennett 1994). During the MCO, global mean annual air temperatures (MAATs) were ~3–5°C warmer than present due to elevated atmospheric carbon dioxide levels of ~600 ppm and consequential changes in deep-ocean circulation and associated meridional heat transfer (e.g. Flower & Kennett 1994, Herold *et al.* 2012). The diverse fossil assemblages preserved in the lacustrine units, including *Nothofagus* (southern beech) wood and leaves, are now absent from Antarctica, suggesting that the warmer climate allowed tundra-like ecosystems to occupy the region until *c.* 14 Ma during the final stage of the MMCT (e.g. Lewis & Ashworth 2015). The MMCT marked the initial step of a progressive cooling in Antarctica and a switch to hyper-arid polar conditions in the upper MDV. Based on a study of meteoric ^{10}Be, it was suggested that no meteoric water has not infiltrated the permafrost sediments for at least the past 14 Myr (Valletta *et al.* 2015).

Considering that the Friis Hills contain a sediment sequence deposited at a time when Earth experienced a major change in climate conditions, the Friis Hills Drilling Project (FHDP) was undertaken in 2016–17 to recover the complete ~50 m-deep mid-Miocene sediment sequence. The sedimentological and stratigraphic description of the cores, including palaeomagnetic measurements, ^{40}Ar/^{39}Ar dating and palaeoenvironmental indicators such as macrofossils, diatoms and pollens, are reported in Chorley *et al.* (unpublished). The objective of this study is to understand the origin and evolution of ground ice in a ~50 m permafrost column over *c.* 15 Myr. This objective is accomplished by investigating the cryostratigraphy of the permafrost sediments, including characterizing the cryostructures and determining the ground ice content, major soluble ions and δD-δ^{18}O composition of the ground ice. This permafrost sequence from the upper MDV provides a unique opportunity to investigate the ground ice conditions of arguably the oldest permafrost on Earth and offers insights into the dynamics of ground ice processes in relation to climate change since the MMCT and the transition to a cold and hyper-arid climate.

Study area

Friis Hills (77°45'S, 161°30'E) is a 12 km-wide inselberg situated at the head of Taylor Valley at 1200–1500 m a.s.l. and ~50 km from the Ross Sea coast (Fig. 1). The local geology of Friis Hills consists of an assemblage of Ordovician and Jurassic age intrusive igneous rocks and Devonian sedimentary rocks of the Beacon Supergroup (Lewis & Ashworth 2015). The multiple advances and retreats of a local alpine glacial system connected to the East Antarctic Ice Sheet deposited a ~50 m-thick sequence of glacial drifts interbedded with lacustrine sediments (Lewis & Ashworth 2015, Chorley *et al.* in preparation). The five FHDP cores consist of a succession of sedimentary facies ranging from subglacial (e.g. diamictites) to fluvial-deltaic (e.g. interstratified, graded or cross-stratified sandstones and/or mudstones) to ice-distal lacustrine environments (e.g. massive mudstones). The ^{40}Ar/^{39}Ar dating of tephras found at the base of core FHDP2C (5.15 m) and at 27.2 m depth in core FHDP3A indicates that the sequence dates between 15 and 14 Ma (Hemming & Cox, personal communication 2020), which is in the upper range of the ages reported by Lewis & Ashworth (2015) and corresponds to the Friis II drift.

Friis Hills is currently located within the stable upland micro-climatic zone where maximum air temperatures remain < 0°C, resulting in little or no melting of snow and/or ice (Marchant & Head III 2007). Dry permafrost extends from the surface to a depth of ~30–35 cm, and the depth of the ice table is largely controlled by ground surface temperature and relative humidity conditions (Fisher *et al.* 2016). A 5 year (2011–15) climate record collected from an automated weather station in Friis Hills (77°44'50.64"S, 161°30'58.32"E, 1591 m a.s.l.) reported a MAAT of -22.7 ± 1.3°C and a mean annual relative humidity of 61.8 ± 5.4% (Doran & Fountain 2019). Measurements on ground temperatures are lacking but based on the absence of a surface offset in the upper MDV (Lacelle *et al.* 2016), the mean annual ground surface temperature should approximate the MAAT.

The sediments at Friis Hills have experienced *c.* 15 Myr of climate change and associated effects on ground thermal and stress regime. Global palaeotemperature reconstructions since the MMCT suggest a general cooling trend until the Holocene punctuated with warm intervals such as the mid-Pliocene (*c.* 3 Ma), when temperatures were ~2–3°C warmer than today (e.g. McKay *et al.* 2012). Since the mid-Pleistocene climate transition (*c.* 1.0–0.8 Ma), Antarctic ice sheets have kept their present cold polar state and sea ice remained permanent in the Ross Embayment, even during warm intervals such as Marine Isotope Stage 5e (MIS5e; *c.* 130–115 ka; Naish *et al.* 2010). Reconstructions of the palaeogeography of the site since the mid-Miocene remain poorly constrained. Early estimates in uplift rates suggest that the Friis Hills region was near sea level during the

https://doi.org/10.1017/S0954102020000619 Published online by Cambridge University Press

Table I. Values of parameters used in REGO ensemble modelling ($n = 36$).

Parameter	Component	Values (n)	Experiment #1
MAT (K)	Thermal	1	250
T_{amp} (K)	Thermal	1	20
GRAD (K 100 m^{-1})	Thermal	1	2
DIFUST (m^2 yr^{-1})	Thermal	2	30, 62
Kpaterson	Creep	1	3
KTENSE	Stress	1	0
KTENS (VdW)	Stress	1	1
LINE (#) (fig. 1 in Fisher *et al.* 2019)	Permeability	1	6
Hamaker constant	Permeability	1	-6.32E-18
R_{soil} (μm)	Mean soil particle radius	3	1, 10, 100
S_{Lthrsh}	Liquid water threshold for VdW forces	2	0.17, 0.13
FDIN	Porosity	2	0.42, 0.5
KSOIL	Soil types used	1	Fujinomori
KBASE	Base water chemistry	1	Seawater
FRACTB	Base chemistry strength fraction	1	0.1

Note: For further explanation of the variables and methods, see Fisher *et al.* (2019).
VdW = Van der Waals.

period of sediment deposition (~100 m Myr^{-1} uplift rate; Fitzgerald 1992); conversely, the latest large-scale palaeotopographical reconstructions based on 3D flexural modelling suggest that the region experienced < 300 m uplift since the Miocene (e.g. Paxman *et al.* 2019). Recent models also estimate that sea level increased by ~30–36 m during the mid-Miocene (Gasson *et al.* 2016) and, assuming minimal uplift, the distance from the Ross Sea coast could have still been reduced to < 20 km. Cores drilled at the mouth of Taylor Valley (DVDP 10 and 11) contained marine deposits, suggesting fjord-like conditions in lower Taylor Valley during the warmer periods of the late Miocene and/or early Pliocene (Porter & Beget 1981) and that similar conditions could have prevailed during the MCO.

Methods

Field sampling

The FHDP cores were collected during the summer of 2016–17 with the objective of recovering the complete 50 m-deep stratigraphic sequence. During coring, sediments in some sections of cores were too dry (unconsolidated by ice) and could not be recovered as a continuous core; the 50 m stratigraphic sequence was recovered by coring in nearby locations. Overall, five cores were combined to provide a stratigraphic sequence from the top of the ice table to 50.48 m depth: FHDP1A (0.86–7.24 and 15.15–33.60 m), FHDP1B (14.59–16.33 m), FHDP2A (0.61–7.05 and 10.40–17.83 m), FHDP2C (0.35–5.18 m) and FHDP3A (15.02–50.48 m). In addition, 12 samples from the surficial dry permafrost at sites FHDP1 and FHDP2 were collected at 1–3 cm intervals. All cores and samples were shipped frozen in thermally insulated boxes to the GNS Ice Core Facility (Wellington, New Zealand), where they were kept frozen at -28°C until being processed for analyses.

Cryostratigraphy and ground-ice content

The sampling of the permafrost cores was based on the sedimentological facies. The lacustrine and glaciofluvial deposits were sampled at high resolution (<1 m intervals), whereas the diamict sections were sampled at 1 m intervals. When present, ice-rich layers were also sampled. The near-surface core FHDP2C was selected for detailed analyses because of its high ground ice content, and it was sampled at 2–5 cm intervals. The cores were sliced using a tile cutter with a 2.2 mm blade and placed into polyethylene bags. All samples were thawed, transferred into pre-weighted and well-sealed graduated polypropylene tubes and, once the sediment settled, the volume of supernatant water and the volume of sediment were recorded. The tubes were then centrifuged to extract the water within the sediment for geochemical analyses. Despite the 273 samples, only 33 samples contained sufficient meltwater for geochemical analyses; 28 samples were from the uppermost 2 m of cores FHFP1A, 2A and 2C and five samples were retrieved from 35–45 m depths in FHDP3A. Once the water was extracted, the sediments were dried at 85°C for 48 h and the mass of the dried sample recorded. Ground ice content was assessed by determining the excess ice, gravimetric water content (GWC) and volumetric ice content (VIC) using equations from Van Everdingen (1998).

Major soluble ion contents

Melted ground ice samples were analysed for major cations (Ca^{2+}, Mg^{2+}, Na^{+}, K^{+}) and anions (Cl^{-}, SO_4^{2-}, NO^{3-}) at the

https://doi.org/10.1017/S0954102020000619 Published online by Cambridge University Press

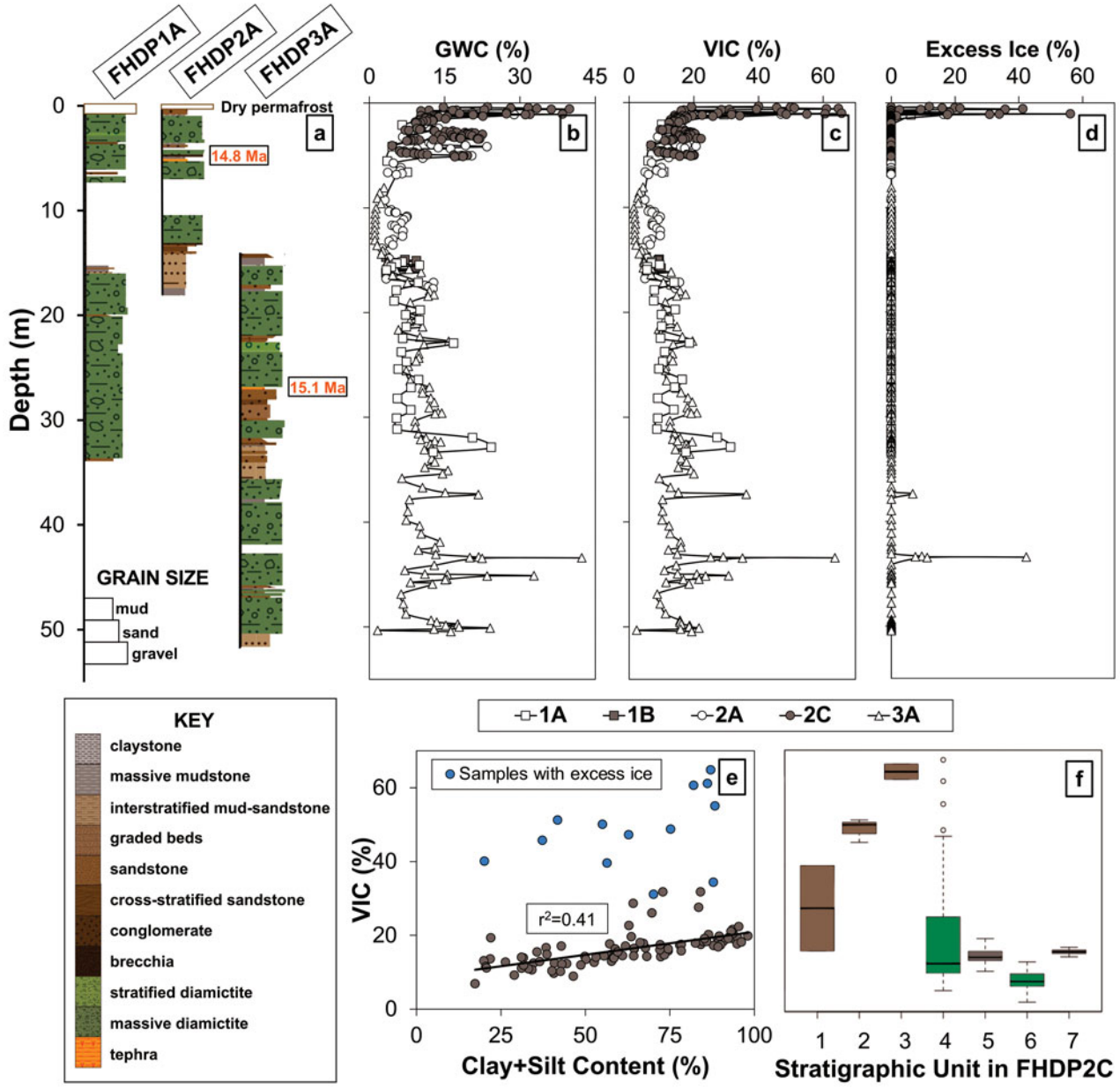

Fig. 2. a. General stratigraphy of Friis Hills Drilling Project (FHDP) cores FHDP1A, 2A and 3A with tephra ages provided by Hemming S. Cox (personal communication 2020). **b.–d.** Gravimetric water content (GWC), volumetric ice content (VIC) and excess ice content, respectively in the five FHDP cores. **e.** Relation between VIC and clay + silt content in FHDP2C. **f.** Boxplots of the VIC for the various stratigraphic units in FHDP2C.

Geochemistry Laboratory, University of Ottawa. The cation samples were first acidified with ultra-pure HNO_3 acid to pH = 2 and analysed using a Varian Vista-Pro inductively coupled plasma atomic emission spectrometer (ICP-AES). The anions were analysed unacidified by ion chromatography using a Dionex-100 device. Analytical reproducibility was ± 5%. To compare samples with different ice contents, the measured concentrations were normalized to the mass of dry soils (mg g^{-1}). The median charge balance for the near-surface samples was of -3.5%, and it was +8.26% for the deeper samples, suggesting that dissolved inorganic carbon, such as HCO_3^- and CO_3^{2-}, were not major missing ions.

Stable water isotopes

The stable water isotopes ($\delta^{18}O$ and δD) of the melted ground ice samples were analysed with a Los Gatos Research (LGR) Triple Isotope Water Analyzer (TIWA-45-EP) coupled to a CTC LC-PAL autosampler

https://doi.org/10.1017/S0954102020000619 Published online by Cambridge University Press

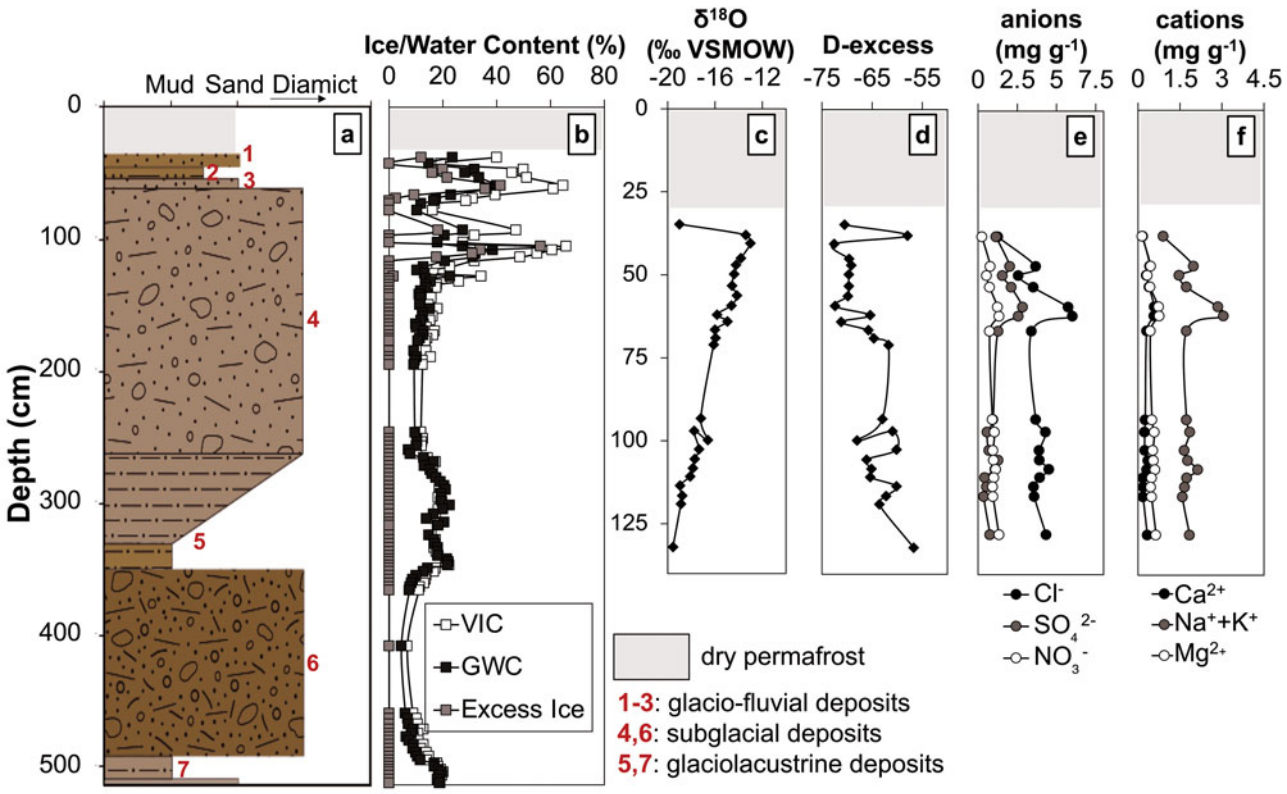

Fig. 3. Sedimentary, ground ice, $\delta^{18}O$ and D-excess and major ion profiles in core FHDP2C. **a.** Lithological facies (described in text and pictured in Fig. S1) including Munsell colours of each unit. **b.** Ground ice content (volumetric ice content (VIC), gravimetric water content (GWC) and excess ice content). **c.** $\delta^{18}O$ composition of ground ice. **d.** D-excess composition of ground ice. **e.** Dissolved anions (Cl^-, SO_4^{2+}, NO_3^-). **f.** Dissolved cations (Ca^{2+}, Na^+, K^+, Mg^{2+}). Note, analyses of stable water isotopes and soluble ions was only possible in the uppermost 1.25 m, where sufficient meltwater could be recovered. VSMOW = Vienna Standard Mean Ocean Water.

for simultaneous $^{18}O/^{16}O$ and D/H ratio measurements and verified for spectral interference contamination. The results are presented using the δ notation ($\delta^{18}O$ and δD), where δ represents the parts per thousand differences for $^{18}O/^{16}O$ or D/H in a sample with respect to Vienna Standard Mean Ocean Water (VSMOW). Analytical reproducibility values for $\delta^{18}O$ and δD were ± 0.3‰ and ± 1‰, respectively. The D-excess was calculated using the equation of Dansgaard (1964): D-excess = $\delta D - 8 \times \delta^{18}O$.

The REGO model

The evolution of an initial ground-ice profile in the 50 m sediment sequence was assessed using the REGO model and its WATERREGO subroutine (Fisher *et al.* 2020a, 2020b). The model allows for evolving residual unfrozen water, including its chemistry and its freezing-point temperature, under changing soil temperature and water-ice phase changes, and the unfrozen water can migrate in the icy soils by diffusive and advective transport driven by stress fields over diurnal and seasonal temperature cycles. The modelling also includes the effect of Van der Waals (VdW) forces that are effective at moving unfrozen water in the uppermost 1 m. The model uses a modified Rempel-type equation to determine the fraction of residual volume of water in freezing soils; however, during the freezing of water at a given temperature decrement, ions are concentrated in the residual water and the new ionic concentration can produce a freezing-point temperature that may be lower than the surrounding soil temperature. This produces an instability in the equation that would force the ground ice to completely melt, but REGO limits the amount of ground ice that can melt based on a heat energy exchange (see eq. (12) in Fisher *et al.* 2020a). The model then combines the results of many possible values of parameters related to soil types, thermal properties and temperature cycles and makes ensemble averages of bulk water speeds, their derivatives with depth and the unfrozen water content at different time steps. The model was intended to produce ensemble average profiles that could be compared to the average profiles of a large suite of boreholes in permafrost in varying terrain (10 or more). In the case of Friis Hills, the number of boreholes is small and they are close together, but the modelling results are nonetheless informative. The model inputs are listed in

https://doi.org/10.1017/S0954102020000619 Published online by Cambridge University Press

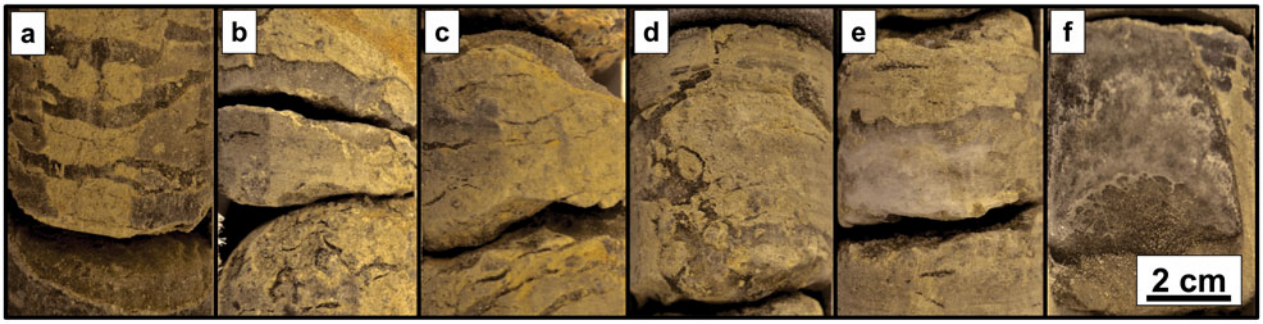

Fig. 4. Examples of lenticular cryostructures in Friis Hills sediments. **a.–e.** Within the upper 1 m of icy permafrost in core FHDP2C. **f.** At 43 m depth in core FHDP3A (section of the 15 cm-thick ice lens).

Table I and are representative of the environmental conditions at Friis Hills.

Results

Sedimentological description of cores

The five FHDP cores provided a 50 m sediment sequence ranging from 0.2–13.3 m-thick layers of massive/stratified diamicts with clasts (subglacial deposits) to 0.1–4.2 m-thick layers of interstratified, graded or cross-stratified sands and/or muds (glaciofluvial deposits) and 0.1–1.5 m-thick layers of massive muds (lacustrine deposits) (Fig. 2a). The 5.15 m-long FHDP2C core that was analysed in detail for cryostratigraphy contained seven stratigraphic units that included 0.02–0.20 m-thick fluvial-deltaic deposits (stratigraphic units 1, 2 and 3), 0.24–1.95 m thick subglacial deposits (stratigraphic units 4 and 6) and 0.62–1.47 m thick lacustrine deposits (stratigraphic units 5 and 7; Fig. 3a). The Munsell colours of the sediments were all within the 2.5Y hue group, alternating mostly between light grey (2.5Y 7/2) and light yellowish brown (2.5Y 6/3) (Fig. 3a). Tephra layers found near the base of core FHDP2C and at 27.2 m depth in core FHDP3A provided preliminary $^{40}Ar/^{39}Ar$ ages from volcanic glass between 15 and 14 Ma (Fig. 2a).

Cryostratigraphy, major ions and δD-δ^{18}O of ground ice

The moisture content in the dry permafrost was lowest at the surface (3%vol.) and increased towards the ice table (30 cm depth), where it reached 10%vol. Below the ice table, the ground ice content in the icy permafrost was consistent between the five cores and showed a general decrease with depth (Fig. 2b–d). The ground-ice content was highest in the uppermost 1 m, where it averaged 29%vol., classifying this interval as ice-rich sediments; ice lenses 0.2–3.0 cm thick were also observed in this interval (Fig. 4a–e). The VIC progressively decreased between 1 and 5 m (from ~23 to 10%vol.) and the cryofacies changed to ice-poor sediment (Figs 2b–d & 3b). Between 5 and 20 m, the VIC was lowest and had values comparable to the surface layer of dry permafrost (2–10%vol.). Below 20 m, the average VIC ranged from 13

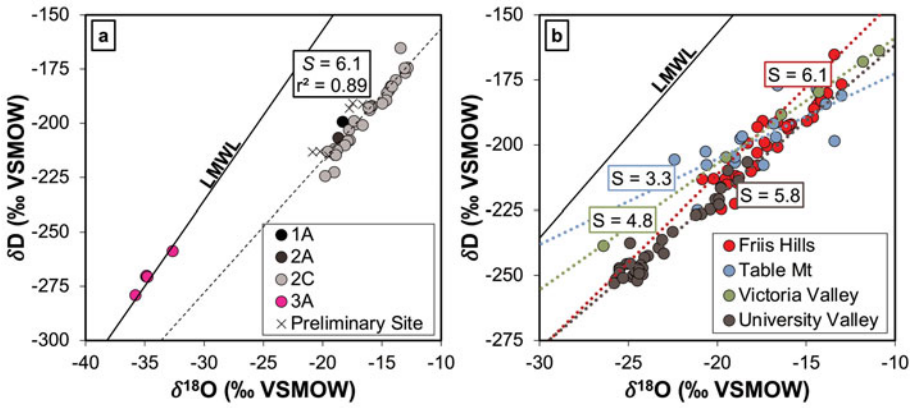

Fig. 5. a. δD-δ^{18}O scatter plot of ground ice in the various cores at Friis Hills. **b.** δD-δ^{18}O of ground ice in core FHDP2C compared with other sites in the McMurdo Dry Valleys: Table Mountain (1945 m above sea level (a.s.l.); Dickinson & Rosen 2003), Victoria Valley (450 m a.s.l.; Hagedorn *et al.* 2010) and University Valley (1600–1800 m a.s.l.; Lapalme *et al.* 2017). The local meteoric water line (LMWL) is shown for comparison purposes (LMWL: δD = 7.9 δ^{18}O + 0.8; Lacelle *et al.* 2011). VSMOW = Vienna Standard Mean Ocean Water.

https://doi.org/10.1017/S0954102020000619 Published online by Cambridge University Press

to 21%vol., increasing slightly compared to the overlying material. Two ice lenses (2 and 15 cm thick) were found in the massive diamicts of FHDP3A at 37 and 43 m depths, respectively (Figs 2b–d & 4f). Ground ice was found in all sedimentological facies, with a small positive correlation between ice content and clay-silt content in core FHDP2C (Fig. 2e & f).

The uppermost 1 m of the FHDP cores had a NaCl geochemical facies, and the sum of ions ranged from 3.9 to 14.3 mg g^{-1} dry soil, averaging 8.8 ± 2.5 mg g^{-1} dry soil. The concentrations of individual anions varied between 258 and 6031 mg kg^{-1} dry soil, with $Cl^- > SO_4^{2-} > NO_3^-$ (Fig. 3e). The concentrations of the individual cations varied between 13 and 2998 mg kg^{-1} dry soil, with $Na^+ > Mg^{2+} > Ca^{2+} > K^+$ (Fig. 3f). In the near surface, the ion content generally increased with depth, with maximum contents at 60 and 110 cm depths (Fig. 3e & f). The molar ratios Na/Cl, Ca/Cl, Mg/Cl, SO_4/Cl and NO_3/Cl averaged 0.74 ± 0.11, 0.07 ± 0.02, 0.19 ± 0.01, 0.13 ± 0.08 and 0.14 ± 0.02, respectively. All molar ratios showed a general decrease with depth, except for Mg/Cl and NO_3/Cl, which increased with depth. In FHDP3A (15.02–50.48 m), samples from ground ice at < 30 m had a $CaSO_4$ geochemical facies and statistically lower total ionic concentration ($P < 0.05$) than in the uppermost 1.5 m; the sum of ions ranged from 0.3 to 0.5 mg g^{-1} dry soil, averaging 0.3 ± 0.1 mg g^{-1} dry soil. Concentrations of anions varied between 0.6 and 171.2 mg kg^{-1} dry soil, with $SO_4^{2-} > Cl^- > NO_3^-$. Concentrations of the major cations varied between 2.9 and 71.6 mg kg^{-1} dry soil, with $Ca^{2+} > Na^+ > Mg^{2+} > K^+$. The molar ratios at < 30 m depth were all significantly higher ($P < 0.05$) than in the uppermost 1.5 m, except for NO_3/Cl, which was near 0 due to the low content of NO_3.

The $\delta^{18}O$ values of the ice lenses found within the uppermost 1 m ranged between -19.8‰ and -12.8‰ (average = -16.2 ± 1.8‰) and showed a general decrease with depth (Fig. 3c). The samples were distributed along a regression slope of 6.1 ($r^2 = 0.89$) and plotted below the MDV local meteoric water line (LMWL) of 7.9 (Fig. 5a). The D-excess values ranged between -73.0‰ and -52.9‰ (average = -65.6 ± 4.3‰; Fig. 3d). Due to low ice content in the 1–30 m intervals of the cores, no samples could be retrieved for δD-$\delta^{18}O$ analysis. The ice lenses at < 30 m in core FHDP3A had the lowest $\delta^{18}O$ values, ranging between -35.8‰ and -32.6‰ (average = -34.6 ± 1.2‰; Fig. 5a). These samples were distributed along the LMWL with D-excess values between 2.4‰ and 8.7‰ (average = 6.9 ± 2.6‰).

Discussion

The Friis Hills cores showed four cryostratigraphic units that were independent of sediment types: 1) surficial dry permafrost (0–30 cm), 2) ice-rich to ice-poor permafrost (0.3–5.0 m), 3) near-dry permafrost (5–20 m), and 4) ice-poor to ice-rich permafrost with distinct thin ice layers (20–50 m). The geochemistry and δD-$\delta^{18}O$ also showed contrasting values between the uppermost ice-rich permafrost and the two ice lenses at < 30 m depth. The ground ice in the uppermost 1 m was characterized by NaCl geochemical facies, high solute load (3.9–14.3 mg g^{-1} dry soil) and $\delta^{18}O$ values (-19.8‰ to –12.8‰) and a δD-$\delta^{18}O$ regression slope of 6.1, which is lower than the LMWL. The 2 and 15 cm-thick ice lenses at < 30 m were characterized by $CaSO_4$ geochemical facies, lower solutes load (0.3–0.5 mg g^{-1} dry soil) and $\delta^{18}O$ values (-35.8‰ to -32.6‰) and a δD-$\delta^{18}O$ distributed along the LMWL. Below, we discuss the cryostratigraphy of the Friis Hills cores by comparing the results to those from other sites in the stable uplands zone. To elucidate dominant processes that shaped ground-ice conditions at Friis Hills, we modelled the evolution of ground ice content using the REGO model.

Origin of ground ice in the upper 1 m

Most studies on ground ice in the MDV have been restricted to shallow (< 6 m) permafrost cores (e.g. Dickinson & Rosen 2003, Hagedorn *et al.* 2010, Lacelle *et al.* 2013, Lapalme *et al.* 2017, Swanger 2017). Excluding the burial of glacier ice, two origins for this ground ice have been proposed: 1) vapour-deposited ice, and 2) ice formed from the freezing of evaporated snowmelt (e.g. Dickinson & Rosen 2003, Hagedorn *et al.* 2010, Lacelle *et al.* 2013, Lapalme *et al.* 2017). Vapour-deposited ground ice is typically characterized by: 1) a maximum ice content at the ice table that subsequently gradually decreases with depth, 2) $\delta^{18}O$ and D-excess profiles that both decrease with depth, and 3) δD-$\delta^{18}O$ slope values similar to the LMWL but shifted below it due to low D-excess (in the -48‰ to -27‰ range). By contrast, the freezing of evaporated snowmelt is generally characterized by: 1) variable ground ice content profiles, 2) decreasing $\delta^{18}O$ but increasing D-excess profiles with depth and 3) δD-$\delta^{18}O$ slopes lower than the LMWL with very low D-excess (mostly in the -83‰ to -46‰ range).

The ground ice samples in the uppermost 1 m of Friis Hills had δD-$\delta^{18}O$ and D-excess compositions that are consistent with the freezing of evaporated snowmelt. The δD-$\delta^{18}O$ and D-excess of ground ice in the uppermost 1 m were enriched in $\delta^{18}O$ by ~10‰ with D-excess being ~60–70‰ lower compared to the isotopic composition of snow and glacial ice in Taylor Valley glacier and snow (e.g. Gooseff *et al.* 2006). However, the δD-$\delta^{18}O$ and D-excess of ground ice was in the range of ground ice from Table Mountain (1945 m a.s.l.) and Victoria Valley (450 m a.s.l.; Fig. 5b). Ground ice in the seasonally

https://doi.org/10.1017/S0954102020000619 Published online by Cambridge University Press

Table II. Input parameters for the evaporation isotope model that calculates the stable isotopes of hydrogen and oxygen for snowmelt seeping downwards in summer through salty soil above the ice table. Based on Sofer & Gat (1975), Craig *et al.* (1963) and Craig (1965).

Parameter	Value
Chemistry (0.1× seawater)	
$MgCl_2$ (mol l^{-1})	5.49E-03
NaCl (mol l^{-1})	4.87E-02
$CaCl_2$ (mol l^{-1})	9.53E-04
KCl (mol l^{-1})	1.06E-03
Water isotopes and fractionation factors	
δ^{18}Ow (‰)	-35
δDw (‰)	-270
δ^{18}Ov (‰)	-28 to -26
δDv (‰)	-285 to -253
Resistance at the bulk water surface for ^{18}O	0.189
Resistance at the bulk water surface for D	0.189
Resistance at the H_2O surface to air boundary for ^{18}O	1.032
Resistance at the H_2O surface to air boundary for D	1.016
Dry lag conditions	
Summer temperature in lag above ice table (°C)	0
Relative humidity (%) in lag	90–95

Note: Equilibrium fractionation factor (α) used for temperature ($T = T_{lag}$).
For water equilibrium, T ≥ surface ice set at -25°C in this example.
$\alpha^{18}O = EXP((1137/T^2) - (0.4156/T) - 0.0020667)$ (T in kelvin).
$\alpha D = EXP((24\,844/T^2) - (76.248/T) + 0.052612)$ (T in kelvin).
For ice equilibrium, T < surface ice, 25°C in this example, T in kelvin.
$\alpha^{18}O = EXP(11.839/T - 0.028224)$ (T in kelvin).
$\alpha D = EXP(129.667/T - 0.351366)$ (T in kelvin).

cryotic zone of University Valley (1600–1800 m a.s.l.) has slightly lower δD-δ^{18}O values, but the D-excess and δD-δ^{18}O slope values are in the same range as those in Friis Hills (Fig. 5b & Fig. S2). Therefore, similar to Table Mountain, Victoria Valley and University Valley, the isotopic composition of ground ice in the uppermost 1 m at Friis Hills was probably affected by two distinct processes: 1) infiltration and partial evaporation of snowmelt through the surficial dry permafrost and 2) its subsequent freezing at the ice table and underlying icy permafrost soils.

The composition of δ^{18}O and D-excess in the uppermost 1 m at Friis Hills was modelled using the Craig *et al.* (1963) and Craig (1965) models for isotopic exchange of evaporating water with ambient soil moisture and the isotope salt effect correction of Sofer & Gat (1975). The model predicts the evolution of evaporating meteoric water in the dry sandy soils during the summer season when the dry soil temperature is at or above the eutectic of the pore water (Table II). At FHDP2, the ice-table depth is 35 cm and, according to the ice-table depth and ground surface humidity relation (Fisher *et al.* 2016), the ground surface humidity is estimated at 93% and the soil relative humidity ranged from 90% to 95%. The initial δ^{18}O composition of snow was set at -35‰ (although it does not significantly influence the steady-state isotopic value) and that of soil water vapour was assumed to be in the -26‰ to -30‰ range (similar to those used for University Valley; Lapalme *et al.* 2017). The initial soluble ion concentration was set at 10% of seawater salinity, as measured just under the ice table (even if the average in the uppermost 1 m of icy permafrost is 47% of seawater salinity). In the modelling scenarios, the δ^{18}O of soil water approached a steady-state value that was dependent on the δ^{18}O of soil vapour and humidity (Fig. 6). The modelled δ^{18}O composition of infiltrating snowmelt required in order to match the range of δ^{18}O values measured near the ice table (-13.4‰) was reached by using a soil relative humidity of 90–95% and a δ^{18}O soil vapour of -26‰ to -28‰ after > 10% of the water had evaporated, after which δ^{18}O residual water reached a steady-state value (Fig. 6). The evaporated snowmelt in the dry soil lag with δ^{18}O composition that evolved from -35‰ to -13‰ then set the initial δ^{18}O composition of water that will begin to freeze at and below the ice table to develop the icy permafrost. Freezing of the partially evaporated snowmelt at the ice table and deeper in the icy permafrost imparts a progressive depletion in δ^{18}O in the residual water (and enrichment in D-excess) due to the preferential incorporation of the heavier isotopes in the ice following a Rayleigh-type isotope fractionation, with the extent of fractionation being dependent on the freezing rate and thickness of the boundary layer (Lacelle *et al.* 2011). Considering that the δD-δ^{18}O composition of the ground ice at Friis Hills and its profile in the uppermost 1 m is very similar to other sites in the stable upland zone where ground ice formed from the infiltration and freezing of evaporated snowmelt (Fig. 5b), this suggests that the environmental conditions between the sites are similar and that the ground ice in the near-surface permafrost is dynamic and responding to changes in environmental conditions. This challenges the assumption that Friis Hills has remained 'frozen' since 13.8 Myr with no infiltration of meteoric water in the sediments (Valletta *et al.* 2015). However, similarly to the other locations in the stable uplands, there probably have been short periods when the ground surface temperatures rose above freezing, even for just a few hours, and with appropriate snow cover, sufficient snowmelt was able to infiltrate the dry sediments and reach the ice table at Friis Hills (e.g. Dickinson *et al.* 2012, Lacelle *et al.* 2016).

Origin of ground ice at 35–50 m depth

At Friis Hills, the 2 and 15 cm-thick ice lenses found at 37 and 43 m depths, respectively, in FHDP3A had lower solute loads (average = 0.3 ± 0.1 mg g^{-1}) and were characterized by a $CaSO_4$ geochemical facies, a eutectic point of -0.02°C, δ^{18}O values of -34.6 ± 1.2‰ and a

https://doi.org/10.1017/S0954102020000619 Published online by Cambridge University Press

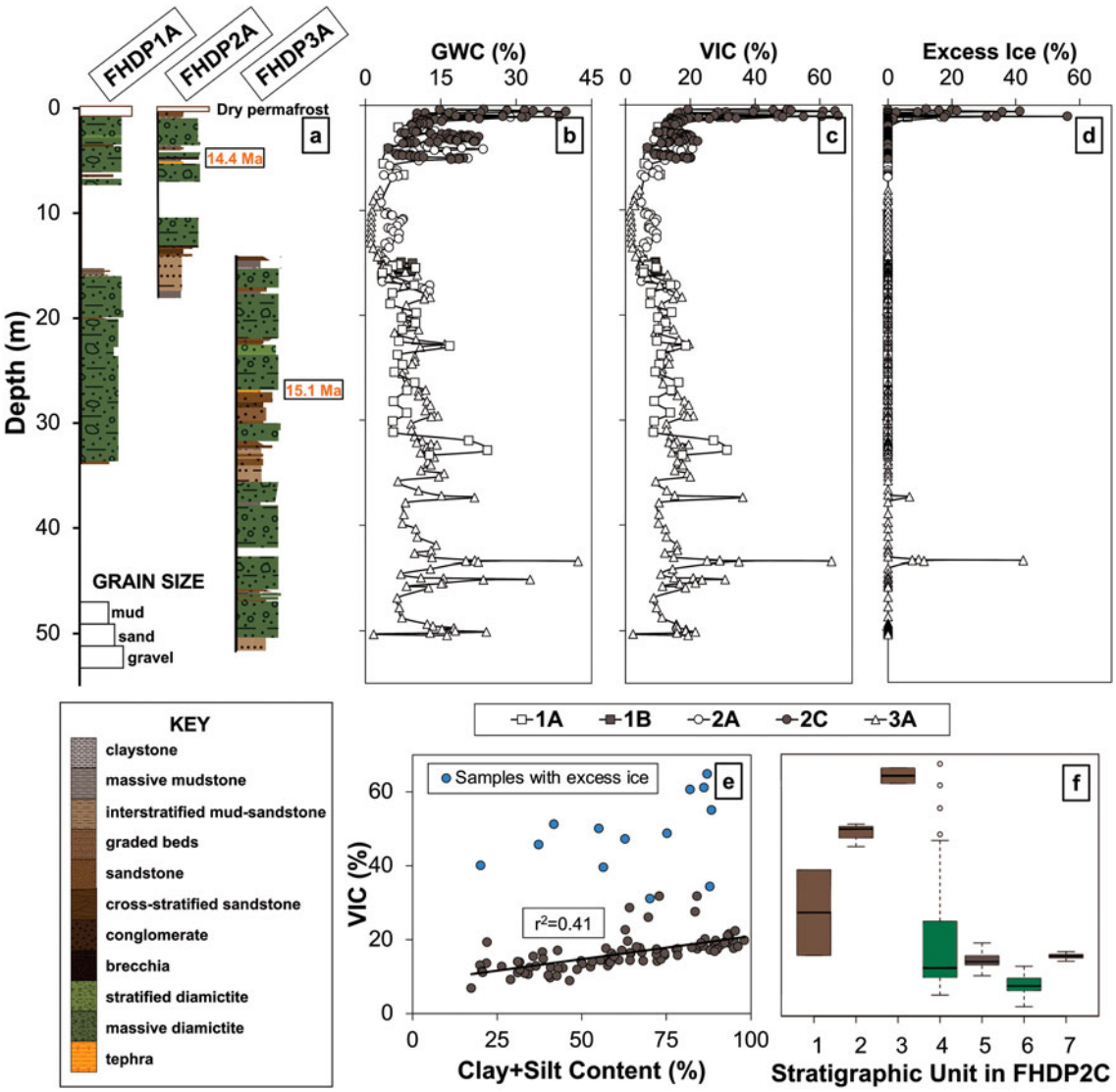

Fig. 6. Evolution of (**a. & c.**) $\delta^{18}O$ and (**b. & d.**) D-excess for two scenarios of relative humidity (RH) (**a. & b.**) of 90% and (**c. & d.**) 95% for a range of soil water vapour values using a combination of the Craig *et al.* (1963) and Craig (1965) models for isotope exchange of evaporating water with ambient soil moisture and the isotope salt effect correction of Sofer & Gat (1975). **e.** At the end of the evaporative evolution, the liquid water $\delta^{18}O$ and δD are used to determine the first formed ice isotopic composition at the ice table. Note, for example, the liquid water's $\delta^{18}O$ at the ice table is ~-15‰, so the first ice formed at the ice table would be ~-12‰ and would progressively decrease with depth following the freezing of the residual water. LMWL = local meteoric water line.

δD-$\delta^{18}O$ regression slope value similar to the LMWL. With the exception of a solute load that was ~ 400 times greater than in precipitation (assuming a 0.74 mg kg^{-1} baseline; Taylor Glacier fresh snow 500 m a.s.l.; Lyons *et al.* 2003), the $\delta^{18}O$ composition, δD-$\delta^{18}O$ slope value and geochemical facies of the deep ground ice are comparable to those of snow and glacial ice located ~20–30 km towards the Ross Sea in the mixed intermediate zone (e.g. lower Taylor Glacier and Canada Glacier; Gooseff *et al.* 2006). Based on these characteristics, it is tempting to associate the deep ice lenses with a buried glacier or snow deposited during the mid-Miocene. However, this origin would not explain the solute load in the ice nor the lenticular cryostructure, which are two characteristics generally associated with intra-sedimental ice (i.e. segregated, injection, intrusive ice; e.g. Coulombe *et al.* 2019 and references therein).

In theory, intra-sedimental ice should have a δD-$\delta^{18}O$ slope value lower than the LMWL, but there are some instances where the δD-$\delta^{18}O$ measurements of this type of ice show a meteoric origin. For example, seasonal ice layers in a pingo near Tuktuyaktuk (Mackay 1990) and reticulate ice in marine clays in the Eureka lowlands (Roy 2019) had δD-$\delta^{18}O$ slope values near the global

https://doi.org/10.1017/S0954102020000619 Published online by Cambridge University Press

meteoric water line (GMWL). The reason as to why the intra-sedimental ice had a δD-δ^{18}O slope near the GMWL, which is similar the FHDP3A ice lenses, relates to sampling and melting the entire ice layer, thus preserving the isotopic mass balance and removing the effect of freezing on δD and δ^{18}O within the ice lens. Considering that the ice lenses preserved a GMWL signature, this suggests that the water from which the deep ice layers formed did not experience evaporation, which would have enriched the δD and δ^{18}O composition prior to freezing and shifted their δD-δ^{18}O composition below the LMWL. This implies that the site probably had an active layer with near-saturated soils, as commonly found today in high Arctic permafrost regions, and not a dry permafrost lag. Therefore, we suggest that the FHDP3A ice lenses originated from the freezing of meteoric water following the deposition of the sediments *c.* 15.0 Ma and probably consist of segregated ice. However, without dating the ice lenses directly, we cannot infer whether the ice is synchronous to the time of sediment deposition *c.* 14–15 Ma, when a tundra ecosystem occupied the region, or during the colder MMCT.

Mid-Miocene palaeotemperature reconstruction

Ice wedges, and more recently pore ice, with δ^{18}O compositions that preserve a meteoric signature are sometimes used as palaeotemperature proxies (e.g. Porter & Opel 2020). In a similar fashion, we can compare the average δ^{18}O composition of the deep ice lenses (-34.6 ± 1.2‰), which probably formed from the freezing of meteoric water, to the 150 000 year record at Taylor Dome (2365 m a.s.l. and 80 km inland) in order to constrain air temperatures during the MCO-MMCT. The δ^{18}O of the ice lenses is 2–3‰ higher than recorded during warm intervals over the past 150 000 years (i.e. early Holocene and MIS5e, which were 1–3°C warmer than today in Antarctica; Grootes *et al.* 2001, Jouzel *et al.* 2007), which, based on the δ^{18}O-temperature relation (dT/d δ^{18}O = 2.1 ± 0.2K/‰), would imply that temperatures at Friis Hills were 5–9°C warmer during the mid-Miocene. However, comparison of late Quaternary climate to that of the mid-Miocene must account for different environmental factors, such as changes in δ^{18}O of seawater, the seasonality of precipitation, distance from coast, site elevation and δ^{18}O-temperature relation. Based on the δ^{18}O of benthic foraminifera, the δ^{18}O of the Southern Ocean during the mid-Miocene was ~1‰ lower than today (Billups & Schrag 2002). In the MDV, the δ^{18}O composition of shallow ice cores on glaciers decrease as a function of distance from the coast, and the data fit the following equation: $y = -0.1528x - 28.38$ ($r^2 = 0.89$; Gooseff *et al.* 2006). The modern δ^{18}O-elevation relation in Antarctica fits a slope of -0.68‰ per 100 m (Wang *et al.* 2009); however, the relation is largely temperature dependent, as shown in Greenland, where the δ^{18}O-elevation relation decreases to -0.62 ± 0.03‰ per 100 m (Dahl-Jensen *et al.* 2013). If we correct the δ^{18}O of ice layers for changes in δ^{18}O of seawater (-1‰) and the latest palaeogeographical conditions of Friis Hills (~30 km closer to the coast due to higher sea level, present-day location of Lake Bonney, +4.5‰ distance from coast; Lyons *et al.* (2005) with little elevation change since the mid-Miocene (0‰), the δ^{18}O composition of the ice would increase by ~3‰ and suggest that the MAAT during the late stage of the mid-Miocene was ~7°C warmer than today. If we keep the same corrections for both δ^{18}O of seawater and distance from coast, but apply 300 m of uplift since the late Miocene (~2‰ uplift; e.g. Wilch *et al.* 1993), the δ^{18}O composition of the ice would increase by ~5‰ and suggest that the MAAT during the late stage of the mid-Miocene was ~11°C warmer than today, corresponding to a MAAT of between -16°C and -11°C (in the range of that in present-day high Arctic Canada). However, this comparison must be taken with caution, as the various δ^{18}O empirical relations cannot be directly transferred to other climate periods because their calibration assumes similar distributions of precipitation, moisture source and trajectory (i.e. unchanged atmospheric circulation; Sturm *et al.* 2010). The MCO and MMCT were periods characterized by changes in deep-ocean circulation and associated meridional heat transfer, therefore most probably affecting moisture source and precipitation (e.g. Herold *et al.* 2012).

A model for ground ice content evolution since the mid-Miocene

The Friis Hills cores showed four cryostratigraphic units: 1) surficial dry permafrost (0–30 cm), 2) ice-rich to ice-poor permafrost (0.3–5.0 m), 3) near-dry permafrost (5–20 m), and 4) ice-poor to ice-rich permafrost with distinct thin ice layers (20–50 m). We have shown that the ground ice in the near-surface is derived from the freezing of evaporated snowmelt and its migration into the icy permafrost, whereas the ground ice in the deep icy permafrost is interpreted to be derived from the freezing of meteoric water. However, the presence of near-dry permafrost across the 5–20 m depth is enigmatic, as both freezing of evaporated snowmelt and vapour diffusion are expected to incorporate ice in accumulating dry sediment (e.g. Fisher *et al.* 2016). For example, even if we ignore the infiltration, migration and freezing of evaporated snowmelt, the slow process of vapour-deposited ice is expected to fill the pore space of sediments with ice within a few hundred years (e.g. Lacelle *et al.* 2013). Through the *c.* 14 Myr of exposure time at Friis Hills, it is possible that the *superimposed*

https://doi.org/10.1017/S0954102020000619 Published online by Cambridge University Press

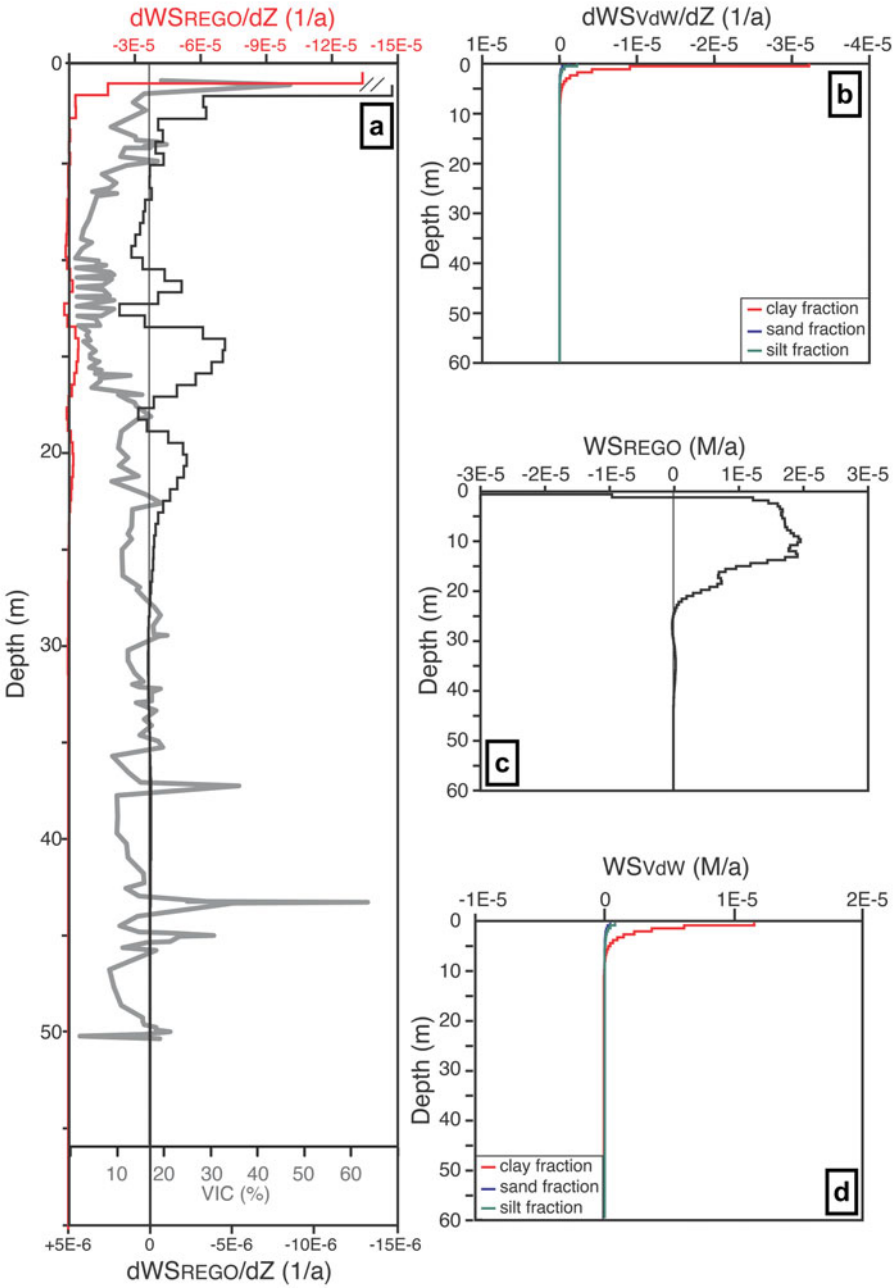

Fig. 7. Comparison of ground ice content profile at Friis Hills with the REGO model. **a.** The depth derivative of the REGO forces residual water speeds plotted in relation to volumetric ice content (VIC) with depth in Friis Hills cores (grey line). Note that because of the enhanced effect of Van der Waals (VdW) forces in the upper 1 m, the depth derivative of the REGO forces within the top 1 m is shown by the red curve and that below is shown by the black curve (both with their separate *x*-axes). **b.** The depth derivative of the VdW forces for different grain sizes. **c.** The ensemble annual average water speed caused by stresses in the icy soils (WS REGO) and by **d.** the VdW forces (WS VdW), respectively. The soil used was the Fujinomori soil (Watanabe & Mizoguchi 2002) and the migrating water started as 1/10th strength seawater (Table I). Fujinomori soil has a clay, silt and sand composition similar to the Friis Hills cores.

ice, which refers to the initial emplacement of ice, evolved to *inherited* ice, which developed from subsequent variations in the initial structure caused by the thermal and stress fields in the icy permafrost. Such redistribution was inferred by Fisher *et al.* (2020a), where the ground ice content profile was predicted to evolve over the Holocene due to the migration of residual unfrozen water in the permafrost under thermal and stress fields. This process results in the development of ice-rich and ice-poor zones at distinct depths

https://doi.org/10.1017/S0954102020000619 Published online by Cambridge University Press

determined by the thermal diffusivity of the icy permafrost, with the change in ice content determined by evolved time.

Here, we use the REGO model with the WATERREGO subroutine to assess how an initial ground-ice profile in a 60 m icy permafrost column would evolve over time under diurnal and seasonal thermal variations using values of input parameters that are representative of the environmental conditions at Friis Hills (Table I). The modelling indicates that the diurnal stress cycles affect the uppermost 30–50 cm and the seasonal stress cycles extends to a depth of ~22 m. This is slightly below the depth of zero thermal amplitude, because stress in a rigid frozen soil can propagate further than the temperature waves that cause them. The diurnal and seasonal thermal regime and associated VdW and rheological forces on the transport of residual water lead to the evolution of ice-rich zones near the surface of permafrost and at 3 and 5 m, as observed in the Friis Hills measurements (Fig. 7). Because of the effectiveness of VdW forces at moving unfrozen water, the uppermost 1 m of icy permafrost is a fast-responding zone, and this could explain why the results from different sites in the MDV have similar ground ice and $\delta^{18}O$ profiles, as they can quickly respond to changing environmental conditions (Fig. S2). From ~5 to 15 m depths, the seasonal cycles and rheological forces remove ice (wet removal process), with the unfrozen water being transported and frozen above or below these depths. This matches fairly well the observed near-dry permafrost at 5–20 m, and the depth difference can be attributed to the simplified stratigraphy in the model (single sediment type and not multi-layered), which would affect the values of the thermal diffusivity. Below the effects of the stresses caused by decaying thermal amplitude (~22 m), the wet removal process has no effect, and the emplaced ground ice is only very slowly modified by upward migration of unfrozen water along the geothermal gradient. The two ice lenses at 37 and 45 m depths occur below the depth of zero thermal and stress amplitudes and would not be modified by the seasonal temperature and stress fields that induce the downwards migration of unfrozen water.

Conclusions

Based on the results presented in this study, the following conclusions can be drawn regarding the cryostratigraphy of Friis Hills and the origin of the ground ice:

- The Friis Hills cores showed four cryostratigraphic units that are independent of sediment types: 1) surficial dry permafrost (0–30 cm), 2) ice-rich to ice-poor permafrost (0.3–5.0 m), 3) near-dry permafrost (5–20 m) and 4) ice-poor to ice-rich permafrost with distinct thin ice layers (20–50 m).
- The ground ice in the uppermost 1 m is characterized by NaCl geochemical facies, high solute loads (3.9–14.3 mg g^{-1} dry soil) and $\delta^{18}O$ values (-19.8‰ to -12.8‰) and a δD-$\delta^{18}O$ regression slope of 6.1, plotting below the LMWL. This indicates that the near-surface ground ice in the ice-rich to ice-poor permafrost (0.3–5.0 m) formed from the freezing of evaporated snowmelt. This process occurs on a regional scale in the MDV (Table Mountain, 1945 m a.sl., Victoria Valley, 450 m a.s.l. and University Valley, 1600–1800 m a.s.l.).
- The near-dry permafrost across 5–20 m depths originates from the redistribution of unfrozen water through rheological forces driven by seasonal thermal and stress fields. This allows for the ground ice content to be slowly removed across that depth over 14 Myr.
- The ground ice at < 30 m is characterized by $CaSO_4$ geochemical facies, lower solute loads (0.3–0.5 mg g^{-1} dry soil) and $\delta^{18}O$ values (-35.8‰ to -32.6‰) and δD-$\delta^{18}O$ distributed along the LMWL. These ice lenses probably formed from the freezing of meteoric groundwater, as shown by their lenticular structure and high salt load in comparison to snow and glacial ice, although a buried snow/ice origin remains a possibility.
- The deep ice lenses and their meteoric signatures suggest a near-saturated active layer following sediment depositions during the mid-Miocene, similar to modern high Arctic sites, where evaporation in the active layer is limited. Temperature reconstruction based on the corrected $\delta^{18}O$ value of the deep ground ice and changes in palaeogeography suggest that the MAAT during the mid-Miocene was ~7–11°C warmer at Friis Hills.

Supplemental materials

Two supplemental figures and eight supplemental tables can be found at https://doi.org/10.1017/S0954102020000619.

Acknowledgements

We would like to thank A. Pyne, R. Pyne and Webster Drilling (T. Kingan and A. Rutten) for retrieving and logging the cores. Special thanks are given to N. Bertler for allowing us to use the GNS Ice Core Facility to store and sample the permafrost cores and A. Philips for welcoming us to use the GNS Science Stable Isotope Laboratory as a transition facility. Laboratory work was made possible with the help of the technical staff at the Sedimentology and Water Quality Laboratory at the Victoria University of Wellington (J. Chewings), the Geography Laboratory at the University of Ottawa (J. Bjornson) and the Geochemistry Laboratory at the University of Ottawa (N. De Silva and S. Mohanty). We

would also like to thank the two reviewers for their constructive comments.

Author contributions

MV, WD and DL designed this project. DL and DF created the WATERREGO and REGO models and generated model outputs. MV, WD, DL, KN and DF contributed to data analysis/interpretation and writing the manuscript. RL and TN developed the Friis Hills Drilling Project. Along with HC, they also retrieved the cores and described the sedimentology of the cores. All authors edited the whole manuscript.

Financial support

The Friis Hills Drilling Project (summer 2016–17) was funded by the Past Antarctic Climate Programme. Funding support was provided by the New Zealand Ministry of Business, Innovation and Employment through contracts C05X1001 and ANTA1801. Fieldwork was made possible with the logistical support of Antarctica New Zealand.

References

Billups, K. & Schrag, D.P. 2002. Paleotemperatures and ice volume of the past 27 Myr revisited with paired Mg/Ca and $^{18}O/^{16}O$ measurements on benthic foraminifera. *Paleoceanography*, **17**, 3–1.

Coulombe, S., Fortier, D., Lacelle, D., Kanevskiy, M. & Shur, Y. 2019. Origin, burial and preservation of late Pleistocene-age glacier ice in Arctic permafrost (Bylot Island, NU, Canada). *The Cryosphere*, **13**, 10.5194/tc-13-97-2019.

Craig, H. 1965. The measurement of oxygen isotope paleotemperatures. *In* Tongiorgi, E., *ed. Stable isotopes in oceanographic studies and paleotemperatures*. Pisa: V. Lischi, 161–182.

Craig, H., Gordon, L. & Horibe, Y. 1963. Isotopic exchange effects in the evaporation of water: 1. Low-temperature experimental results. *Journal of Geophysical Research*, **68**, 10.1029/JZ068i017p05079.

Dahl-Jensen, D., Albert, M., Aldahan, A., Azuma, N., Balslev-Clausen, D., Baumgartner, M., Berggren, A.-M., *et al.* 2013. Eemian interglacial reconstructed from a Greenland folded ice core. *Nature*, **493**, 10.1038/nature11789.

Dansgaard, W. 1964. Stable isotopes in precipitation. *Tellus*, **16**, 436–468.

Dickinson, W.W. & Rosen, M.R. 2003. Antarctic permafrost: an analogue for water and diagenetic minerals on Mars. *Geology*, **31**, 10.1130/0091-7613(2003)031<0199:APAAFW>2.0.CO;2.

Dickinson, W.W., Schiller, M., Ditchburn, B.G., Graham, I.J. & Zondervan, A. 2012. Meteoric Be-10 from Sirius Group suggests high elevation McMurdo Dry Valleys permanently frozen since 6 Ma. *Earth and Planetary Science Letters*, **355**, 10.6073/pasta/9dda244e95ce8dfcdbd9b94d2289ef1d.

Doran, P. & Fountain, A. 2019. McMurdo Dry Valleys LTER: Daily measurement summaries from Friis Hills Meteorological Station (FRSM) in Taylor Valley, Antarctica from 1993 to present ver 6. *Environmental Data Initiative*, 10.6073/pasta/4c19209bd0cc73f5b30d6b98eca47bc9.

Fisher, D., Lacelle, D. & Pollard, W. 2020a. A model of unfrozen water content and its transport in icy permafrost soils: effects on ground ice content and permafrost stability. *Permafrost and Periglacial Processes*, **31**, 10.1002/ppp.2031.

Fisher, D.A., Lacelle, D., Pollard, W. & Faucher, B. 2020b. A model for stable isotopes of residual liquid water and ground ice in permafrost soils using arbitrary water chemistries and soil-specific empirical residual water functions. *Permafrost and Periglacial Processes*, 10.1002/ppp.2079.

Fisher, D., Lacelle, D., Pollard, W., Davila, A. & McKay, C.P. 2016. Ground surface temperature and humidity, ground temperature cycles and the ice table depths in University Valley, McMurdo Dry Valleys of Antarctica. *Journal of Geophysical Research - Earth Surface*, **121**, 10.1002/2016JF004054.

Fitzgerald, P.G. 1992. The Transantarctic Mountains of southern Victoria Land: the application of apatite fission track analysis to a rift shoulder uplift. *Tectonics*, **11**, 10.1029/91TC02495.

Flower, B.P. & Kennett, J.P. 1994. The middle Miocene climatic transition: East Antarctic ice sheet development, deep ocean circulation and global carbon cycling. *Palaeogeography, Palaeoclimatology, Palaeoecology*, **108**, 10.1016/0031-0182(94)90251-8.

Fountain, A., Fernandez-Diaz, J.C., Obryk, M.K., Levy, J., Gooseff, M.N., van Horn, D.J., *et al.* 2017. High-resolution elevation mapping of the McMurdo Dry Valleys, Antarctica, and surrounding regions. *Earth System Science Data*, **9**, 10.5194/essd-9-435-2017.

Grootes, P.M., Steig, E.J., Stuiver, M., Waddington, E.D., Morse, D.L. & Nadeau, M.J. 2001. The Taylor Dome Antarctic ^{18}O record and globally synchronous changes in climate. *Quaternary Research*, **56**, 289–298.

Gasson, E., DeConto, R.M., Pollard, D. & Levy, R.H. 2016. Dynamic Antarctic ice sheet during the early to mid-Miocene. *Proceedings of the National Academy of Sciences of the United States of America*, **113**, 10.1073/pnas.1516130113.

Gooseff, M.N., Lyons, W., McKnight, D.M., Vaughn, B.H., Fountain, A.G. & Dowling, C. 2006. A stable isotopic investigation of a polar desert hydrologic system, McMurdo Dry Valleys, Antarctica. *Arctic, Antarctic, and Alpine Research*, **38**, 10.1657/1523-0430(2006)038[0060:ASIIOA]2.0.CO;2.

Hagedorn, B., Sletten, R.S., Hallet, B., McTigue, D.F. & Steig, E.J. 2010. Ground ice recharge via brine transport in frozen soils of Victoria Valley, Antarctica: insights from modeling $\delta^{18}O$ and δD profiles. *Geochimica et Cosmochimica Acta*, **74**, 10.1016/j.gca.2009.10.021.

Herold, N., Huber, M., Müller, R. & Seton, M. 2012. Modeling the Miocene Climatic Optimum: ocean circulation. *Paleoceanography*, **27**, 10.1029/2010PA002041.

Jouzel, J., Masson-Delmotte, V., Cattani, O., Dreyfus, G., Falourd, S., Hoffmann, G., *et al.* 2007. Orbital and millennial Antarctic climate variability over the past 800,000 years. *Science*, **317**, 10.1126/science.1141038.

Lacelle, D., Davila, A.F., Pollard, W.H., Andersen, D., Heldmann, J., Marinova, M. & McKay, C.P. 2011. Stability of massive ground ice bodies in University Valley, McMurdo Dry Valleys of Antarctica: using stable O-H isotope as tracers of sublimation in hyper-arid regions. *Earth and Planetary Science Letters*, **301**, 10.1016/j.epsl.2010.11.028.

Lacelle, D., Lapalme, C., Davila, A.F., Pollard, W., Marinova, M., Heldmann, J. & McKay, C.P. 2016. Solar radiation and air and ground temperature relations in the cold and hyper-arid Quartermain Mountains, McMurdo Dry Valleys of Antarctica. *Permafrost and Periglacial Processes*, **27**, 10.1002/ppp.1859.

Lacelle, D., Davila, A.F., Fisher, D., Pollard, W.H., DeWitt, R., Heldmann, J., *et al.* 2013. Excess ground ice of condensation-diffusion origin in University Valley, Dry Valleys of Antarctica: evidence from isotope geochemistry and numerical modeling. *Geochimica et Cosmochimica Acta*, **120**, 10.1016/j.gca.2013.06.032.

Lapalme, C., Lacelle, D., Pollard, W., Fisher, D., Davila, A. & McKay, C.P. 2017. Distribution and origin of ground ice in

University Valley, McMurdo Dry Valleys, Antarctica. *Antarctic Science*, **29**, 10.1017/S0954102016000572.

Lewis, A.R. & Ashworth, A.C. 2015. An early to middle Miocene record of ice-sheet and landscape evolution from the Friis Hills, Antarctica. *Bulletin*, **128**, 10.1130/B31319.1.

Lyons, W., Welch, K.A., Fountain, A.G., Dana, G.L., Vaughn, B.H. & McKnight, D.M. 2003. Surface glaciochemistry of Taylor Valley, southern Victoria Land, Antarctica and its relationship to stream chemistry. *Hydrological Processes*, **17**, 10.1002/hyp.1205.

Lyons, W., Welch, K.A., Snyder, G., Olesik, J., Graham, E.Y., Marion, G.M. & Poreda, R.J. 2005. Halogen geochemistry of the McMurdo Dry Valleys lakes, Antarctica: clues to the origin of solutes and lake evolution. *Geochimica et Cosmochimica Acta*, **69**, 305–323.

Mackay, J. 1990. Seasonal growth bands in pingo ice. *Canadian Journal of Earth Sciences*, **27**, 10.1139/e90-116.

Marchant, D. & Head III, J.W. 2007. Antarctic dry valleys: microclimate zonation, variable geomorphic processes, and implications for assessing climate change on Mars. *Icarus*, **192**, 10.1016/j.icarus.2007.06.018.

Marinova, M.M., McKay, C.P., Pollard, W.H., Heldmann, J.L., Davila, A.F., Andersen, D.T., *et al*. 2013. Distribution of depth to ice-cemented soils in the high-elevation Quartermain Mountains, McMurdo Dry Valleys, Antarctica. *Antarctic Science*, **25**, 10.1017/S095410201200123X.

McKay, C.P., Mellon, M.T. & Friedmann, E.I. 1998. Soil temperatures and stability of ice-cemented ground in the McMurdo Dry Valleys, Antarctica. *Antarctic Science*, **10**, 31–38.

McKay, R., Naish, T., Carter, L., Riesselman, C., Dunbar, R., Sjunneskog, C., *et al*. 2012. Antarctic and Southern Ocean influences on late Pliocene global cooling. *Proceedings of the National Academy of Sciences of the United States of America*, **109**, 10.1073/pnas.1112248109.

Naish, T., Wolff, E., Carter, L., McKay, R. & Powell, M. 2010. Antarctic climate evolution during the Quaternary (last 2.6 Ma) from continental margin, Southern Ocean and ice core records. *Quaternary International*, **219**, 10.1016/j.quaint.2010.02.006.

Paxman, G.J., Jamieson, S.S., Hochmuth, K., Gohl, K., Bentley, M.J., Leitchenkov, G. & Ferraccioli, F. 2019. Reconstructions of Antarctic topography since the Eocene-Oligocene boundary. *Palaeogeography, Palaeoclimatology, Palaeoecology*, **535**, 10.1016/j.palaeo.2019.109346.

Porter, S. & Beget, J.E. 1981. Provenance and depositional environments of late Cenozoic sediments in permafrost cores from lower Taylor Valley, Antarctica. *Dry Valley Drilling Project*, **33**, 10.1029/AR033p0351.

Porter, T. & Opel, T. 2020. Recent advances in paleoclimatological studies of Arctic wedge- and pore-ice stable-water isotope records. *Permafrost and Periglacial Processes*, **31**, 10.1002/ppp.2052.

Roy, C. 2019. *The origin of massive ground ice in raised marine sediments along the Eureka Sound Lowlands, Nunavut, Canada*. PhD thesis, McGill University [Unpublished], 122 pp.

Sofer, Z. & Gat, J. 1975. The isotope composition of evaporating brines: effect of the isotopic activity ratio in saline solutions. *Earth and Planetary Science Letters*, **26**, 10.1016/0012-821X(75)90085-0.

Sturm, C., Zhang, Q. & Noone, D. 2010. An introduction to stable water isotopes in climate models: benefits of forward proxy modelling for paleoclimatology. *Climate of the Past*, **6**, 10.5194/cp-6-115-2010.

Swanger, K.M. 2017. Buried ice in Kennar Valley: a late Pleistocene remnant of Taylor Glacier. *Antarctic Science*, **29**, 10.1017/S0954102016000687.

Valletta, R.D., Willenbring, J.K., Lewis, A.R., Ashworth, A.C. & Caffee, M. 2015. Extreme decay of meteoric beryllium-10 as a proxy for persistent aridity. *Scientific Reports*, **5**, 17813, 10.1038/srep17813.

Van Everdingen, R.O. 1998. *Multi-language glossary of permafrost and related ground-ice terms*. Ottawa: International Permafrost Association, 159 pp.

Wang, Y., Hou, S., Masson-Delmotte, V. & Jouzel, J. 2009. A new spatial distribution map of $\delta^{18}O$ in Antarctic surface snow. *Geophysical Research Letters*, **36**, 10.1029/2008GL036939.

Watanabe, K. & Mizoguchi, M. 2002. Amount of unfrozen water in frozen porous media saturated with solution. *Cold Regions Science and Technology*, **34**, 103–110.

Wilch, T.I., Lux, D.R., Denton, G.H. & McIntosh, W.C. 1993. Minimal Pliocene-Pleistocene uplift of the dry valleys sector of the Transantarctic Mountains: a key parameter in ice-sheet reconstructions. *Geology*, **21**, 10.1130/0091-7613(1994)022<0668:MPPUOT>2.3.CO;2.